Solar Soft X-ray Irradiance Variability, III: MagneticField Variations of Coronal X-ray Features

Rangaiah Kariyappa

kari.hemi@gmail.com

Indian Institute of Astrophysics

H.N. Adithya

Manipal Centre for Natural Sciences, Manipal Academy of Higher Education

Satoshi Masuda

Institute for Space-Earth Environmental Research (ISEE), Nagoya University

Kanya Kusano

Institute for Space-Earth Environmental Research (ISEE), Nagoya University

Shinsuke Imada

Department of Earth and Planetary Science, The University of Tokyo

Joe Zender

European Space Research and Technology Center (ESTEC)

Luc Dame

LATMOS (Laboratoire Atmosph`eres, Milieux, Observations Spatiales)

Edward DeLuca

Center for Astrophysics Harvard & Smithsonian

Mark Weber

Center for Astrophysics Harvard & Smithsonian

Research Article

Keywords: Sun: X-ray radiation, Sun: corona, Sun: coronal magnetic features, Sun: magnetic fields of coronal features

Posted Date: November 9th, 2023

DOI: https://doi.org/10.21203/rs.3.rs-3571756/v1

Additional Declarations: No competing interests reported.

Version of Record: A version of this preprint was published at Solar Physics on April 11th, 2024. See the published version at https://doi.org/10.1007/s11207-024-02289-9.

Solar Physics
DOI: 10.1007/•••••-•••-•••-••••-•

Solar Soft X-ray Irradiance Variability, III: Magnetic Field Variations of Coronal X-ray Features

Rangaiah Kariyappa[1,2]•• · H.N. Adithya[3] · Satoshi Masuda[2] · Kanya Kusano[2] · Shinsuke Imada[4] · Joe Zender[5] · Luc Damé[6] · Edward DeLuca[7] · Mark Weber[7]

Received Mmm DD, YYYY; accepted Mmm DD, YYYY

Abstract
The magnetic field changes the radiative output of the Sun and is the main source for all the solar surface features. To study the role of the underlying photospheric magnetic field in relation to emission features observed in the solar corona, we have used the full-disk soft X-ray images from Hinode/X-Ray Telescope (Hinode/XRT) and the magnetograms obtained from Helioseismic and Magnetic Imager (HMI) on board the Solar Dynamics Observatory (SDO) for a period of about 13 years (May 2010 – June 2023), which covers the Solar Cycle 24. A sophisticated and established algorithm developed in Python is applied to the X-ray observations from Hinode/XRT to segment the different coronal

✉ R. Kariyappa
rkari@iiap.res.in, kari.hemi@gmail.com

1 Indian Institute of Astrophysics, Bangalore-560034, India

2 Institute for Space-Earth Environmental Research (ISEE), Nagoya University, Nagoya, Japan

3 Manipal Centre for Natural Sciences, Manipal Academy of Higher Education, Manipal 576104, India

4 Department of Earth and Planetary Science, The University of Tokyo, Tokyo 113-0033, Japan

5 European Space Research and Technology Center (ESTEC), 2200 AG Noordwijk, The Netherlands

6 LATMOS (Laboratoire Atmosphères, Milieux, Observations Spatiales),11 boulevard d'Alembert, 78280 Guyancourt, France

7 Harvard-Smithsonian Center for Astrophysics, 60 Garden Street, Cambridge, MA, USA

features by creating segmentation maps of the active regions (ARs), coronal holes (CHs), background regions (BGs), and X-ray bright points (XBPs). Further, these maps are applied to the full-disk (FD) line-of-sight (LOS) magnetograms from HMI to isolate the X-ray coronal features and photospheric magnetic counterparts, respectively. We then computed full-disk and feature-wise averages of X-ray intensity and line of sight (LOS) magnetic flux density (MFD) over ARs/CHs/BGs/XBPs/FD. Variations in the quantities resulting from the segmentation, namely the integrated intensity, temperature from filter ratio method and the integrated magnetic flux density of ARs/CHs/BGs/XBPs/FD regions, are inter-compared, and compared with sunspot number (SSN). We find that the X-ray intensity/temperature over ARs/CHs/BGs/XBPs/FD are well correlated with the underlying magnetic field. We discuss the intensity/temperature/magnetic flux density variations of a full-disk corona and of all the features. The time series plots of the integrated magnetic flux density of the full-disk and all the features (except XBPs) show magnetic flux density fluctuations synchronized with the solar cycle (sunspot number), whereas the fluctuations of the magnetic flux density values in XBPs show a slight anti-phase with SSN. Although the magnetic flux density of all features varies, but the mean magnetic flux density values estimated for the whole observed period of the full-disk is around $8.40\text{x}10^7$ DN and active regions (ARs) are around $1.15\text{x}10^7$ DN, whereas BGs, CHs, and XBPs are $6.50\text{x}10^7$ DN, $0.19\text{x}10^7$ DN, and $0.15\text{x}10^7$ DN, respectively. In addition, we found that the mean magnetic field contribution estimated of the background regions (BGs) will be around 85 %, whereas ARs/CHs/XBPs are 11 %, 2 % and 2 % respectively to the average magnetic flux density of the full-disk. The magnetic field time series of all the features suggest that the features show a high variability in their magnetic field similar to intensity/temperature fluctuations, suggesting that the magnetic field is important in producing the different emission features which are associated with different intensity/temperature values. The magnetic field is responsible for the heating rate of the emission features which are highly variable on solar cycle timescales. We conclude from the full-disk intensity-temperature-magnetogram analysis that the magnetic field plays a crucial role in driving the different brightenings/emissions/temperature and heating of the corona at the sites of these magnetic features. In this study it has been demonstrated that the segmented coronal features observed in the soft X-ray wavelength can be used as proxies to isolate the corresponding underlying magnetic structures.

Keywords: Sun: X-ray radiation – Sun: corona – Sun: coronal magnetic features – Sun: magnetic fields of coronal features

1. Introduction

The magnetic field plays an important role in the solar irradiance variability and in the heating of the solar atmosphere. Segmentation of the full-disk images and determination of the contribution of different magnetic emission features to total magnetic flux variability is equally important issue in solar physics when

we consider the Sun-Earth connection and heliospheric studies in general. Solar magnetic fields are manifested as distinct features on the Sun because their presence cause changes in the radiative output and properties of the solar atmosphere. The active regions are associated with high magnetic fields including the sunspots in the photosphere. In general the intensity of active regions increases monotonically with increasing magnetic flux at the chromospheric and coronal heights.

The spatially resolved full-disk CaII K spectroheliograms show the different chromospheric features such as plages, chromospheric active and quiet network, and bright points which are seen in emission and associated with different levels of intensity and magnetic flux values. Although these features are responsible to produce the chromospheric variability in its radiative output, but it has not been determined, routinely, the detailed relationship between the evolution of magnetic features and solar spectral irradiance variability using full-disk magnetograms and CaII K images. A similar observations have been done in the quiet chromosphere and found that the CaII K-line intensity is well correlated with the absolute value of the magnetic flux density (Skumanich, Smythe, and Frazier, 1975). The chromospheric emission features observed in CaII K-line have one-to-one spatial correspondence with the underlying photospheric magnetic features and hence the magnetic field is responsible for the heating of the chromosphere and its emission features.

In regard to the relationship between the coronal emission features and photospheric magnetic features, it has been compared the integrated full-disk solar X-ray flux with the total unsigned magnetic flux (Pevtsov et al., 2003). They used almost 10-years of soft X-ray data from Yohkoh/SXT space mission and full-disk magnetograms from Kitt Peak Solar Observatory, and found the relationship between them will follow the power law with an index between 1.6 and 2.0. However, the segmentation of all the magnetic features (ARs/CHs/BGs/XBPs) from the full-disk magnetograms and their variability in comparison with solar soft X-ray flux and sunspot number and their contribution variations over the solar cycle have not been studied.

Previously, it has been estimated the contribution of various coronal features to EUV and UV irradiance variability using spatially resolved full-disk observations in EUV and UV wavelengths for the period from 2011 to 2012 from PROBA2/SWAP and SDO/AIA (Kumara et al., 2014). In continuous of this work, we have segmented the EUV and UV full-disk intensity images observed with PROBA2/SWAP (174Å) and SDO/AIA (171Å, 193Å) and full-disk line-of-sight (LOS) magnetograms from SDO/HMI for the period from 2011 to 2016 (Zender et al., 2017). From this investigation, we found that the EUV and UV intensity of ARs/CHs/QS/FD features are well correlated with the corresponding underlying photospheric magnetic elements and concluded that the segmentation of the full-disk solar images and magnetograms are useful in the reconstruction of the solar spectral irradiance (SSI) variations. Recently, we have segmented the different coronal features (ARs/CHs/BGs/XBPs) from the full-disk solar soft X-ray images observed with Hinode/XRT and studied their intensity and area variations for the Solar Cycle 24 (Adithya et al., 2021), Paper I hereafter. Further, we determined the temperature of all these features using the intensity

filter ratio method and investigated the temporal variations of the temperature for the Solar Cycle 24 (Adithya et al., 2023), Paper II, hereafter. So far no attempts have been made to compare the full-disk soft X-ray segmented intensity images with the segmented magnetograms and to extract the corresponding magnetic field of ARs/CHs/BGs/XBPs/FD and to study their variability over the Solar Cycle 24 in comparison with their intensity and temperature. From our Papers I and II, we already have the intensity/temperature values of the various segmented coronal features, using these derived values it would be interesting to estimate and compare the corresponding underlying photospheric magnetic features, and to determine their contribution to integrated magnetic flux and their variability and magnetic role over the Solar Cycle 24.

In this paper, we attempted *for the first time,* to use the segmented intensity/temperature maps to overlie on the full-disk magnetograms and extract the magnetic flux density (MFD) values of the segmented features such as active regions (ARs), coronal holes (CHs), background regions (BGs), and X-ray bright points (XBPs). The following sections discuss the details of the observations, analysis, results of magnetic field and contribution variations of ARs/CHs/BGs/XBPs, and full-disk intensity (FDI) in comparison with their intensity/temperature and sunspot number (SSN).

2. Observations and Analysis

2.1. Observations

We used the data observed from the Helioseismic and Magnetic Imager instrument on board Solar Dynamic Observatory (SDO/HMI) (Hoeksema et al., 2014) and X-Ray Telescope on board Hinode (Hinode/XRT) satellites (Kosugi et al., 2007; Golub et al., 2007). The level 1.5, full-disk, HMI line-of-sight (LOS) magnetograms, 4096x4096 pixels size images have been downloaded from the JSOC data archive for the period May 01, 2010 to June 17, 2023 (Solar Cycle 24). HMI has both a 45-second cadence image for high temporal resolution and a 720-second cadence image for a lower noise level version. We have chosen the 720-second cadence image for this study. The HMI LOS magnetograms are fully corrected for detector, optics, and degradation effects (see for more details: (Couvidat et al., 2016)).

We have considered XRT images of level-2, full-disk, and composite images of size both 2048x 2048 pixels and 1024x1024 pixels. The data has been downloaded from http://solar.physics.montana.edu/HINODE/XRT/SCIA/synop _images/syncmp_FITS, for the same period as HMI. The data already applied with xrt_prep.pro which is standard IDL/SSW routine, corrects for vignetting, subtracts a dark frame, normalizes exposure time and removes high-frequency noise. Further improvisation is done by correcting contamination spots on CCD and pixel saturation and updating satellite jitter correction information (Takeda, Yoshimura, and Saar, 2016).

Out of 8 filters of XRT, we choose Al-mesh filter, which is thin, frequently and regularly observed, it provides high signal-to-noise ratio images throughout

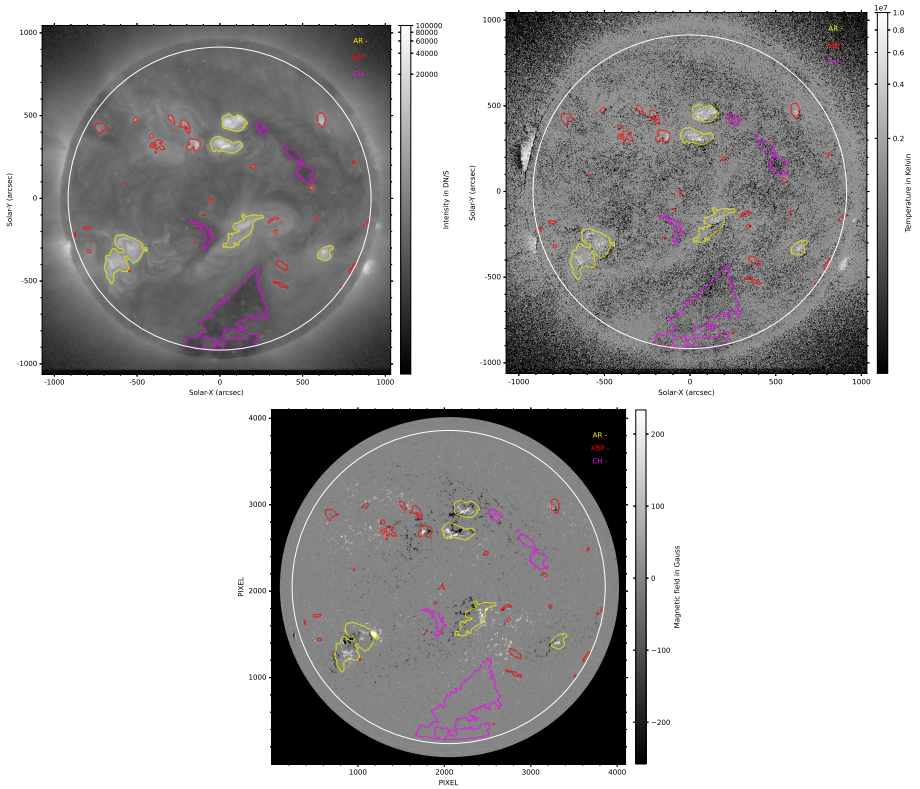

Figure 1. A sample of composite intensity image (top left panel), temperature (top right panel, showing black pixels due to thresholding used in Paper II and log scale used here) and magnetic field (bottom panel) maps observed on March 27, 2012. Maps showing all the features (ARs – Yellow, CHs – Magenta, XBPs – Red and BGs – remaining disk). The white circle on the image is 95% of the radius considered for analysis.

the Solar Cycle 24. A stray light leak issue started to appear in the Al-mesh filter after 2015. The IDL/SSW routine 'xrt_synleaksub.pro' was applied to all the images after 2015 to remove for stray light leak component. In our previous papers I and II, we have discussed in great detail on the corrections applied to the full-disk XRT images to improve the quality of the images and explained the advantages in using the composite images.

2.2. Analysis

In our previous paper (Paper I), we have described the details of segmentation of coronal features such as Active Regions (ARs), Coronal Holes (CHs), Background (BGs), X-ray Bright Points (XBPs) and studied the intensity variation of both full-disk and individual features for the period: February 2007 - March 2020. In our next paper (Paper II) we generated the temperature images of the solar corona using Al-mesh, Ti-poly and Al-poly filters of XRT for the period of February 2008 to June 2021 by filter ratio method. In papers I and II, we

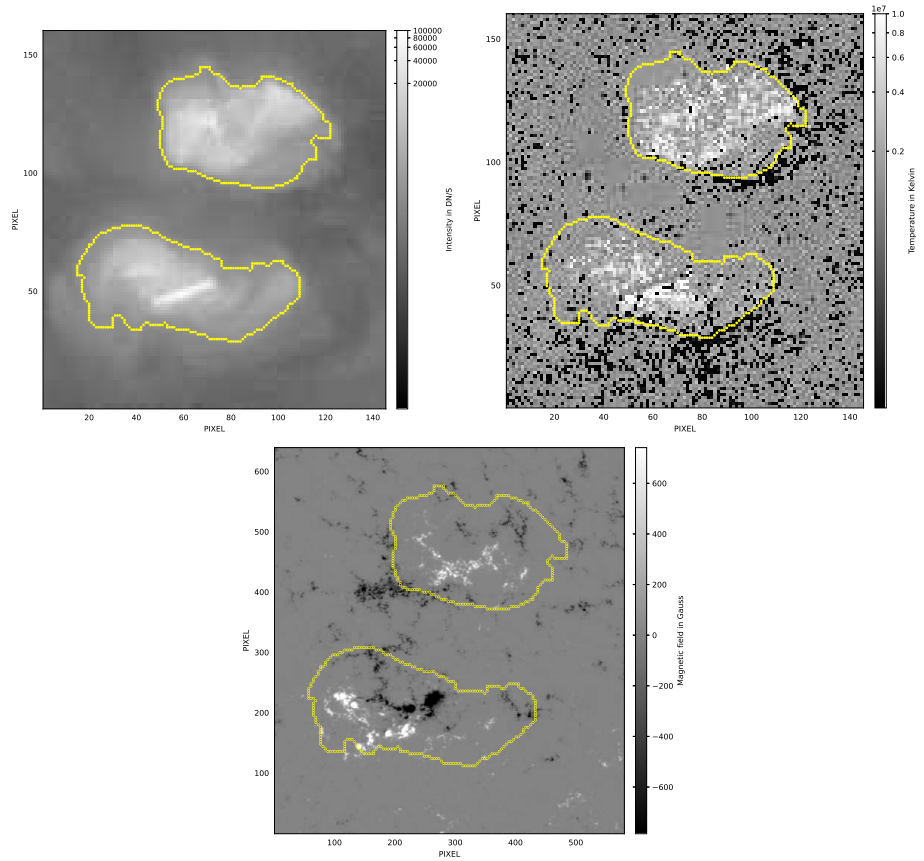

Figure 2. A sample of an active region with the contours in intensity/temperature/magnetic field observed on March 27, 2012. The temperature map showing black pixels due to thresolding used in Paper II and log scale used here.

discussed about the segmentation processes of the coronal features and derived their intensity/temperature values for the Solar Cycle 24.

In this paper, we use the segmentation contours created in Paper I and carefully overlaid on HMI magnetograms and XRT temperature images created in our Paper II to get the magnetic field of coronal features ARs/CHs/BGs/XBPs. In Figure 1, we have shown a sample of a composite intensity image (top left panel), temperature map (top right panel) and magnetic field map (bottom panel) showing all the features (ARs/CHs/BGs/XBPs) obtained on March 27, 2012 from Hinode/XRT and SDO/HMI. In Figure 2, we have shown the contour maps for comparison of an active region observed on March 27, 2012 in intensity/temperature/magnetic field images. We noticed that the contours are identical in all the images suggesting that the algorithm works satisfactorily.

The time series of the magnetic flux density was generated using the following steps:

(i) The segmentation map is generated by segmenting the Al-mesh image as described in our Paper I, and the intensity of the full-disk and of all the features of the image are calculated.

(ii) In our Paper II, we used the filter ratio method to derive the temperature maps. The temperature map showing all the features (ARs/CHs/BGs/XBPs) observed on March 27, 2012 with Hinode/XRT is shown in Figure 1 (right panel).

(iii) The HMI LOS magnetograms are selected which are closest time of observation from XRT.

(iv) Segmentation maps are scaled up based on the solar disc radius on XRT images and magnetograms.

(v) Segmentation maps are aligned to magnetograms and carefully overlaid on it and the integrated magnetic flux density of the ARs/CHs/BGs/XBPs and full-disk (FD) are extracted.

(vi) Similarly, segmentation maps are overlaid on the XRT temperature image and the average temperature of the ARs/CHs/BGs/XBPs/FD are extracted. The time series of intensity/temperature/magnetic flux density of all the features ARs/CHs/BGs/XBPs and full-disk were generated, inter-compared and compared with sunspot number (SSN).

The time series of the magnetic flux density, area and the magnetic contribution values of ARs/CHs/BGs/XBPs/FD have been derived and compared with their intensity/temperature and sunspot number (SSN). The important results of the magnetic field analysis are presented and discussed in the following sections.

3. Results

In our previous paper (Paper I), we discussed the details about: (i) the segmentation of full-disk soft X-ray images, (ii) the algorithm developed in Python to identify and segment coronal X-ray features (ARs/CHs/BGs/XBPs) from the full-disk soft X-ray observations of Hinode/XRT, (iii) the intensity and area of all the features in comparison with GOES (1-8 Å) X-ray flux and sunspot number (SSN), and (iv) the contribution of all the features to total soft X-ray flux variations. In the next paper (Paper II), we have further studied and presented about: (i) the full-disk soft X-ray segmented features observed from Hinode/XRT in different filters for Solar Cycle 24, (ii) the temperature maps of the corona generated using the filter ratio method, (iii) the mean temperature of the features are determined and compared to solar activity, (iv) the average temperature contributions of all the features to total temperature of the full-disk corona. We concluded from Papers I and II that the coronal features are associated with different morphology, brightnesses/intensities, and temperatures. The intensity and temperature of the features show temporal fluctuations on both small timescale and solar cycle timescales. The different intensity/temperature values associated with them may be related to the underlying photospheric magnetic field and the magnetic field may be responsible to produce the different

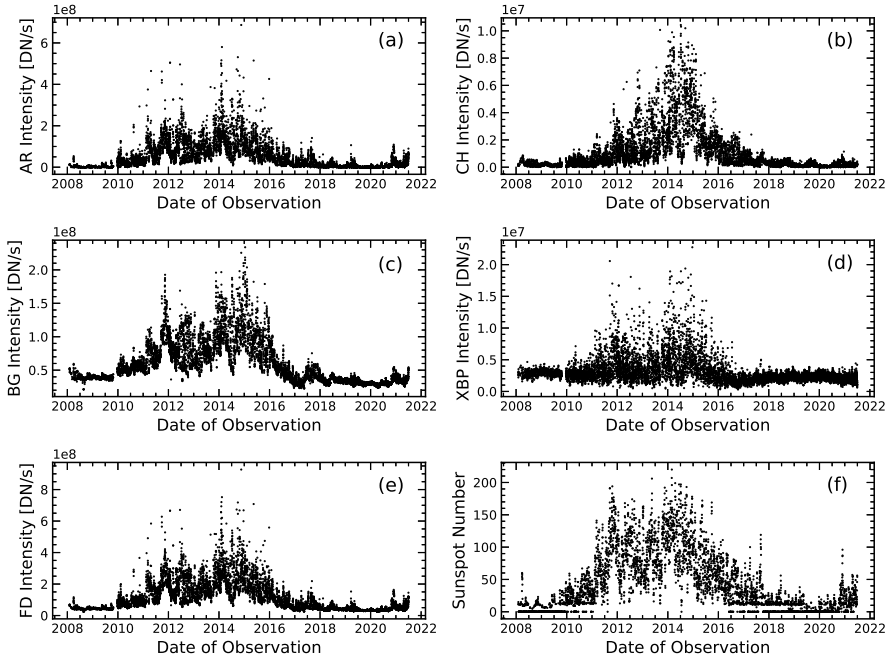

Figure 3. Time series of the total intensity of solar X-ray features: (a) ARs, (b) CHs, (c) BGs, (d) XBPs, (e) full-disk intensity (FDI) (observed in Al-mesh filter from Hinode/XRT), and for comparison with (f) sunspot number (SSN) for a period: February 01, 2008 to June 30, 2021 – Solar Cycle 24 (Figure 2 of Paper I).

brightnesses and temperatures and hence to the heating of the corona at the sites of the coronal features. To address such issues, a detailed analysis of the segmentation of full-disk magnetograms (SDO/HMI) in comparison with the segmented intensity/temperature maps (from Hinode/XRT) is required.

In the present analysis we discuss about: (a) the intensity segmentation maps (Hinode/XRT) overlaid on SDO/HMI magnetograms for the period May 01, 2010 to June 17, 2023 (Solar Cycle 24), (b) determination of the magnetic flux density values of all the coronal features (ARs/CHs/BGs/XBPs) and full-disk, (c) the comparative studies between the intensity/temperature/magnetic field of all the features, (d) the variations of magnetic flux density values of all the coronal features and full-disk are compared with sunspot number (SSN) for the Solar Cycle 24. The important results derived from the full-disk intensity-temperature-magnetogram analysis are presented in detail in the following sections.

3.1. Intensity, Temperature, Magnetic Flux Density and Area Variations of the Coronal Features

In Figures 3 and 4, we have shown the time series of total intensity (derived from Paper I, Figure 2) and temperature (derived from Paper II, Figure 6) of each of the coronal features and full-disk, and the sunspot number (SSN) also plotted

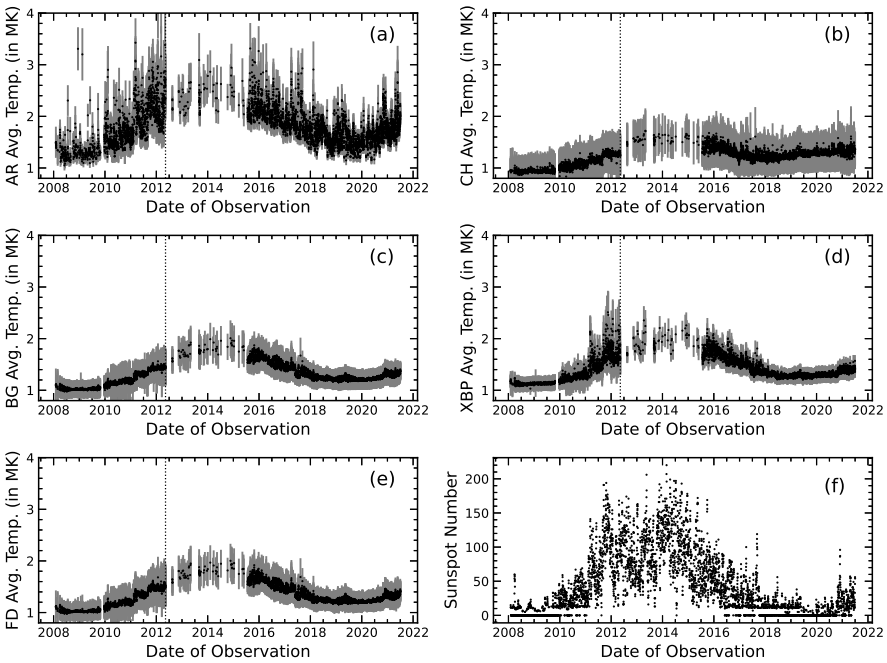

Figure 4. Time series of the total temperature of solar X-ray features: (a) ARs, (b) CHs, (c) BGs, (d) XBPs, (e) full-disk (FD), and for comparison with (f) sunspot number (SSN) for a period: February 01, 2008 to June 30, 2021 – Solar Cycle 24 (Figure 6 of Paper II).

for comparison. The intensity and temperature variations of all the features are discussed in detail in Papers I and II. In this paper, we will be comparing the Figures 3 and 4 with the magnetic flux density values of all the features derived from the SDO/HMI full-disk magnetograms. We estimated the integrated magnetic flux density values of all the features and full-disk and are plotted in Figure 5 for the period: May 01, 2010 to June 17, 2023 along with the sunspot number for the Solar Cycle 24. It is clear from the time series Figures 3, 4, and 5 that the temporal variations of the magnetic flux density values are in phase with the intensity/temperature fluctuations of the features (ARs/CHs/BGs), whereas the magnetic flux density of XBPs are slightly in anti-phase with the fluctuations of intensity/temperature. The intensity/temperature/magnetic flux density values of ARs/CHs/BGs are well synchronized with the sunspot number variations and well correlated each other, whereas the XBPs show a weak anti-correlation with SSN. In Figure 5, we show the temporal variations in average magnetic flux density of all the features, along with the full-disk and compare them with the sunspot number (SSN) for the Solar Cycle 24. The mean magnetic flux density of the full-disk and of all the features show magnetic field variations and they vary with sunspot number (solar activity), except that the magnetic flux density of XBPs show an anti-correlation with SSN. We have normalized the magnetic flux density values with the area by dividing the magnetic flux density with the number of pixels. The normalized magnetic flux density values are plotted

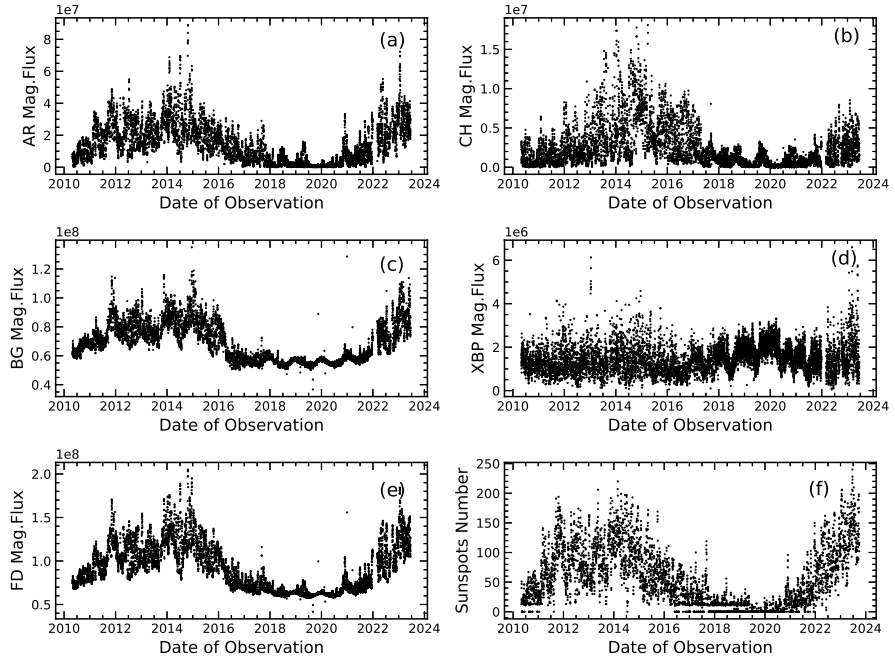

Figure 5. Time series of the integrated magnetic flux density (from SDO/HMI) of solar X-ray features: (a) ARs, (b) CHs, (c) BGs, (d) XBPs, (e) full-disk (FD), and for comparison with (f) sunspot number (SSN) for a period: May 01, 2010 to June 17, 2023 – Solar Cycle 24.

in Figure 6. When we normalize the magnetic flux density values with area, the magnetic flux density values of all the features (ARs/CHs/BGs/XBPs/FD), including the XBPs vary in phase with the sunspot number variations. We noticed the differences between the Figures 5 and 6 that the CHs does not show much variations and XBPs show a positive variations with SSN in Figure 6 when we divide the magnetic flux density values by their area. This is because the total number of XBPs are higher during solar minimum and lower at the solar maximum period (the related detail paper is in preparation). Although the magnetic flux density of all features varies, but the mean magnetic flux density values estimated for the whole observed period of the full-disk is around $8.4\text{x}10^7$ DN and active regions (ARs) are around $1.15\text{x}10^7$ DN, whereas BGs, CHs, and XBPs are $6.5\text{x}10^7$ DN, $0.19\text{x}10^7$ DN, and $0.15\text{x}10^7$ DN, respectively. We conclude from the time series data (Figure 5) that the magnetic field is important for the intensity/temperature fluctuations on longer time scale. It is also clear from Figure 5 that, on an average, over the solar cycle, the integrated magnetic flux density of BGs is larger than the integrated magnetic flux density of ARs/CHs/XBPs, but the contribution of ARs will become more prominent around solar maximum. The extraction of magnetic field of all the features would help to study the relation between the intensity, temperature and the strength of the magnetic field, and how the magnetic field plays a role in driving the different brightenings/emissions and different intensity/temperature values,

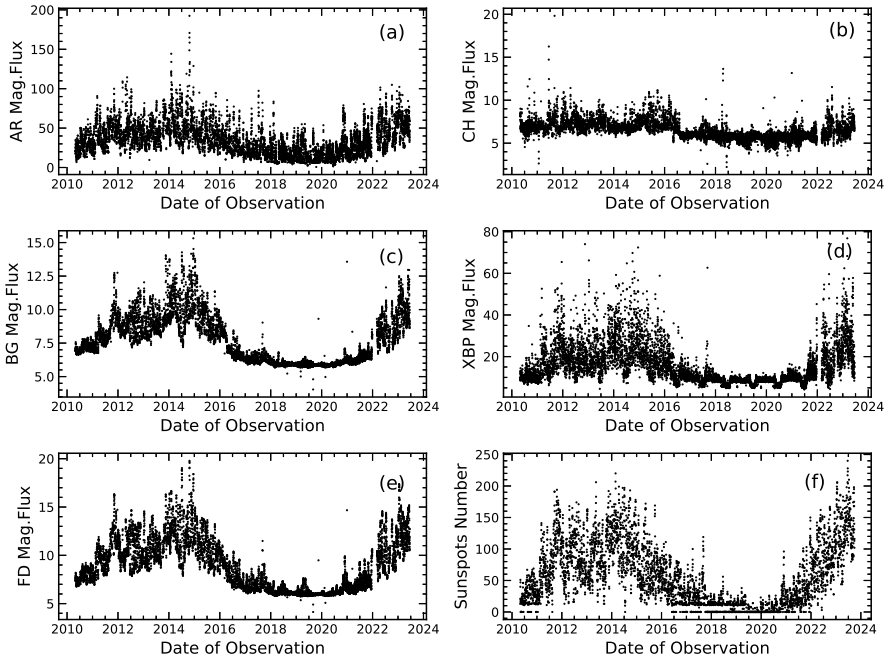

Figure 6. Time series of the integrated magnetic flux density values normalized to area (magnetic flux density/number of pixels) (from SDO/HMI) of solar X-ray features: (a) ARs, (b) CHs, (c) BGs, (d) XBPs, (e) full-disk (FD), and for comparison with (f) sunspot number (SSN) for a period: May 01, 2010 to June 17, 2023 – Solar Cycle 24.

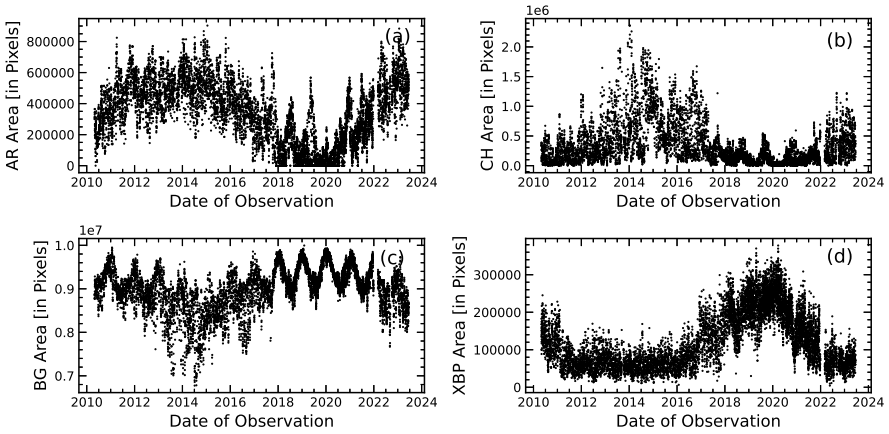

Figure 7. Total area (total number of pixels) variation of the solar X-ray features: (a) ARs, (b) CHs, (c) BGs, and (d) XBPs measured from SDO/HMI full-disk segmented magnetograms for the period: May 01, 2010 to June 17, 2023 – Solar Cycle 24.

Table 1. Spearman rank correlation coefficients between (a) intensity (int) vs. temperature (temp), (b) intensity vs. magnetic flux density (MFD) and (c) temperature vs. magnetic flux density of all coronal features (ARs/CHs/BGs/XBPs) and FDI as observed with Hinode/XRT and SDO/HMI

	Correlation Coefficients (R)		
	Int vs.Temp (Fig.8)	Int vs.MFD (Fig.9)	Temp vs.MFD (Fig.10)
ARs	0.89	0.94	0.88
CHs	0.04	0.71	-0.12
BGs	0.43	0.93	0.62
XBPs	0.64	-0.32	0.72
FDI	0.58	0.97	0.74

and in the heating mechanisms of the corona at the sites of all these features. The combined results of the variations in intensity/temperature/magnetic field associated with the coronal features will help to understand the solar corona and its heating mechanism more clearly and in detail.

In addition to magnetic flux density, we have estimated the total area (total number of pixels) of ARs/CHs/BGs/XBPs for whole period from the segmented magnetogram maps. In Figure 7 we plotted the area of all the features (ARs/CHs/BGs/XBPs) for the whole observed period, and these are compared with the integrated intensity, temperature, magnetic flux density and magnetic flux density/area of all the segmented features and sunspot number variations presented in Figures 3, 4, 5 and 6 respectively. The features' area variation (shown in Figure 7) show that the area of ARs and CHs vary with the solar activity, whereas the BGs and XBPs are anti-correlated with the phase of the solar cycle. It is already observed in the intensity/temperature analysis and detailed in our previous Papers I and II that during solar minimum the areas covered by BGs and XBPs are large compared to the areas of ARs and CHs. A similar behavior has been seen (Figure 7) in the area variations extracted from the segmented magnetogram maps. This represents that the area of the features vary with the solar cycle and area is responsible for the modulation of the magnetic flux density, intensity and temperature values on longer time scales. So, the area of the magnetic features is highly variable similar to intensity/temperature/magnetic flux density values and need to be considered along with other parameters in the reconstruction of solar spectral irradiance (SSI) variability. The variation in magnetic flux density values of all the features suggest that the features show a high variability in their magnetic field and that the heating rate of the emission features may be highly variable on solar cycle timescales.

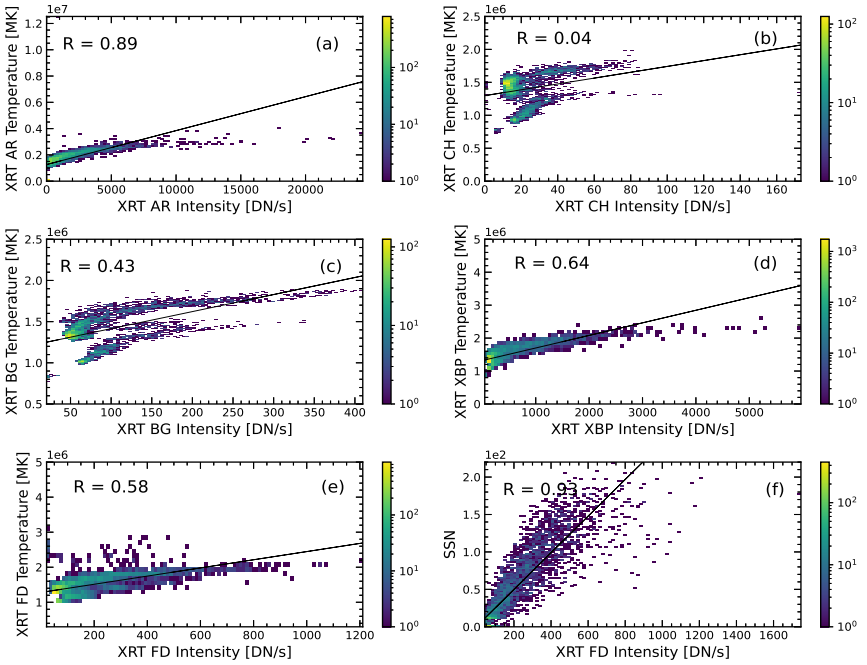

Figure 8. Scatter plots of temperature versus intensity of all the solar X-ray features.

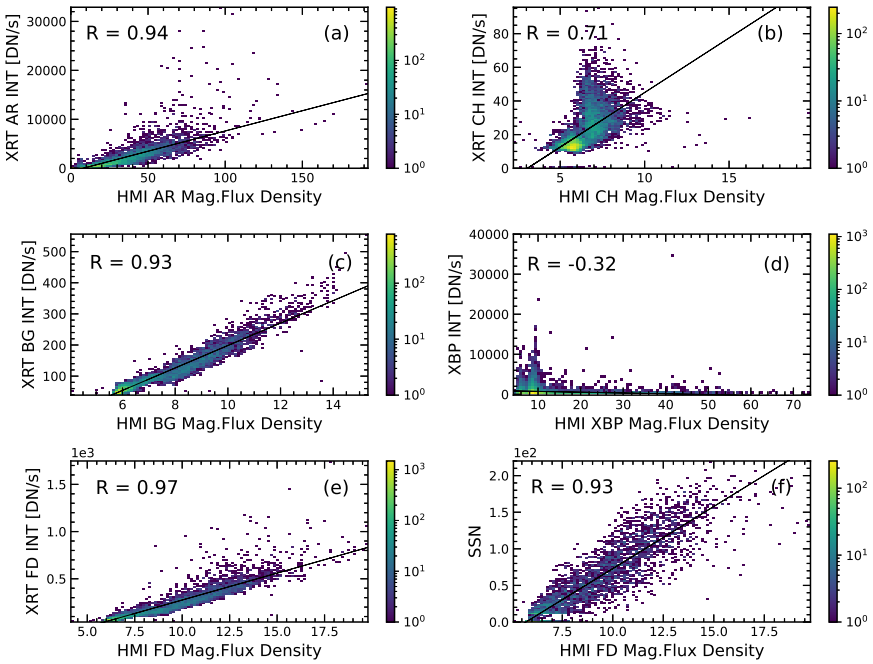

Figure 9. Scatter plots of intensity versus magnetic flux density (normalised to area) of all the solar X-ray features.

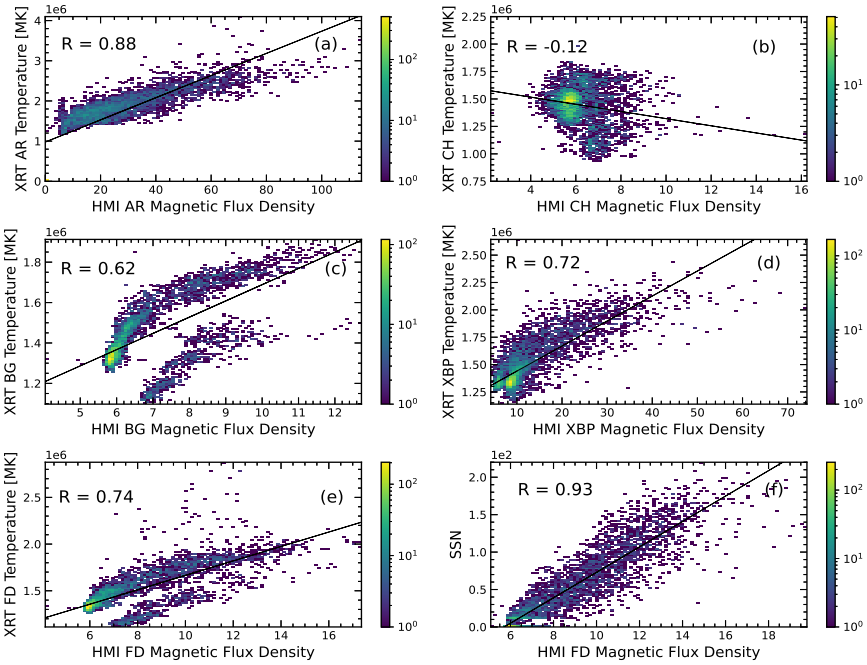

Figure 10. Scatter plots of temperature versus magnetic flux density (normalised to area) of all the solar X-ray features.

3.2. Correlation Analysis between the Intensity, Temperature and Magnetic Field of the Coronal Features

In section 3.1, we observed in the time series of intensity (Figure 3), temperature (Figure 4), magnetic field (Figure 5) and magnetic flux density/area (Figure 6) of all the features are well correlated each other, except the magnetic field variations of XBPs in Figure 5. To understand the relationship between them and for better presentation, we have plotted the intensity versus temperature in Figure 8, intensity versus magnetic flux density (normalised to area) in Figure 9, and temperature versus magnetic flux density (normalized to area) in Figure 10 of all the features including versus SSN. We observed from the scatter plots that all the features (ARs/BGs/FD/SSN) show a good correlation whereas the intensity of CHs is well correlated with magnetic flux density (Figure 9b), but their temperature with MFD (Figure 10b) and intensity with temperature (Figure 8b)) are weakly correlated. Whereas the intensity of XBPs show a good correlation with temperature (Figure 8d), the temperature of XBPs is well related to MFD (Figure 10d) and intensity show weak correlation with MFD (Figure 9d). We worked out the correlation coefficients (R) and are presented in Table 1. We noticed from the Figures 8, 9 and 10 and Table 1 that the R values of all the features for intensity versus the magnetic flux density are higher in general compared to temperature versus the magnetic flux density and intensity versus temperature (R values of Int vs MFD > Temp vs MFD > Int vs

Temp). This implies that the magnetic field is more correlated to intensity than the temperature of the coronal features (ARs/CHs/BGs). The ARs and BGs have strong correlation and correspondence with the underlying photospheric magnetic elements. In addition we observed that the XBPs are also associated with the corresponding magnetic field having a good correlation compared to CHs, indicating that the magnetic field may be the main cause for the brightness oscillations and heating of the XBPs.

It is very surprise to notice that there are two bands or families of data points in some of the scatter plots as shown in: Temp vs Int for CHs (Figure 8b) and Temp vs Int for BGs (Figure 8c). Similarly we obsereved the two bands in Temp vs MFD for BGs (Figure 10c) and Temp vs MFD for FD (Figure 10e) scatter plots. However, the cause for the two bands or families of data points as seen in the scatter plots is unclear and may be further investigations are required. A similar behaviour was reported by (BenMoussa et al., 2013),(Kumara et al., 2014) and (Zender et al., 2017) when they are comparing SWAP integrated intensities against EVE computed intensity and SWAP with AIA intensity values.

3.3. Correlation Analysis between the Magnetic Field of the Coronal Features and Sunspot Number (SSN)

From the time series shown in Figures 3, 4, 5, 6, and 7 we noticed that the integrated intensity, temperature, magnetic flux density values and along with the areas of all the features exhibit the expected 27 day modulation due to the solar rotation, similar to sunspots at the photospheric level. In Figure 11, we have plotted the average magnetic flux density of all the features (ARs/CHs/BGs/XBPs) and the full-disk magnetic flux density versus the sunspot number for the period May 01, 2010 to June 17, 2023, before removing the 27-day modulation. Similar scatter plots of all features versus sunspot number, after removing the 27-day modulation, are shown in Figure 12. To remove the 27-day modulation we have averaged the data points in the time series for every 27 days. The Spearman rank correlation coefficients of the average magnetic flux density of segmented features with sunspot number have been calculated before and after removing the 27-day modulation in the time series data. The corresponding correlation coefficients (R) are tabulated in Table 2. We observed that the R values are higher for the time series after removing the 27-day oscillation. This implies that the resulting correlations for each feature are due to the solar cycle itself and that the magnetic flux density time series are in phase with the sunspot number time series. It suggests that the changes in magnetic flux density of all the coronal features are more dependent on long-term solar cycle variations than the 27-day oscillations. In addition, we noticed that even the magnetic flux density/area of all the features are also more dependent on long-term solar cycle variations than the 27-day modulations. A similar results have been reported in the temperature analysis (Paper II). As seen from the scatter plots (Figures 11 and 12) and the results of the correlation coefficients (presented in Table 2), the average magnetic flux density of all features are well correlated with sunspot number, except the XBPs. The spatially resolved images are an important and valuable asset for understanding of the magnetic field, intensity and temperature

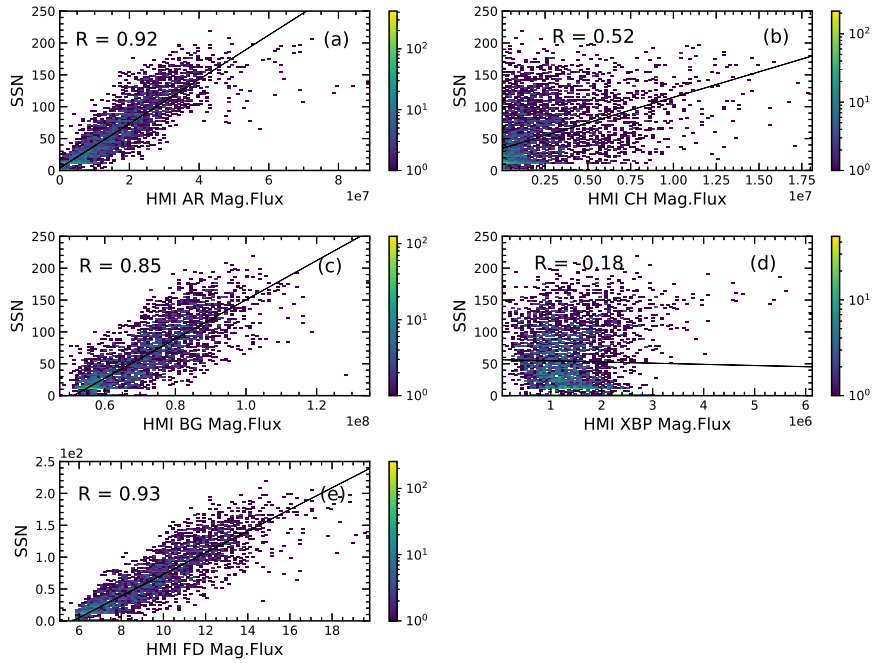

Figure 11. Total magnetic flux density of all the features: (a) ARs, (b) CHs, (c) BGs, (d) XBPs, and (e) FDT are plotted versus SSN for the period: May 01, 2010 to June 17, 2023 – before removing 27-day modulation.

variabilities of the Sun when we observe the Sun as a Star. In that case, the Sun can be used as a calibrator to measure the integrated magnetic field of any solar-type stars.

Table 2. Spearman rank correlation coefficients (before and after removing the 27-day modulation) between sunspot number (SSN) and the average magnetic flux density of coronal features (ARs/CHs/BGs/XBPs) and FDI as observed with SDO/HMI

	Correlation Coefficients (R)	
	Before removing 27-day modulation (Fig.11)	After removing 27-day modulation (Fig.12)
ARs vs SSN	0.92	0.97
CHs vs SSN	0.52	0.70
BGs vs SSN	0.85	0.90
XBPs vs SSN	-0.18	-0.16
FDI vs SSN	0.93	0.96

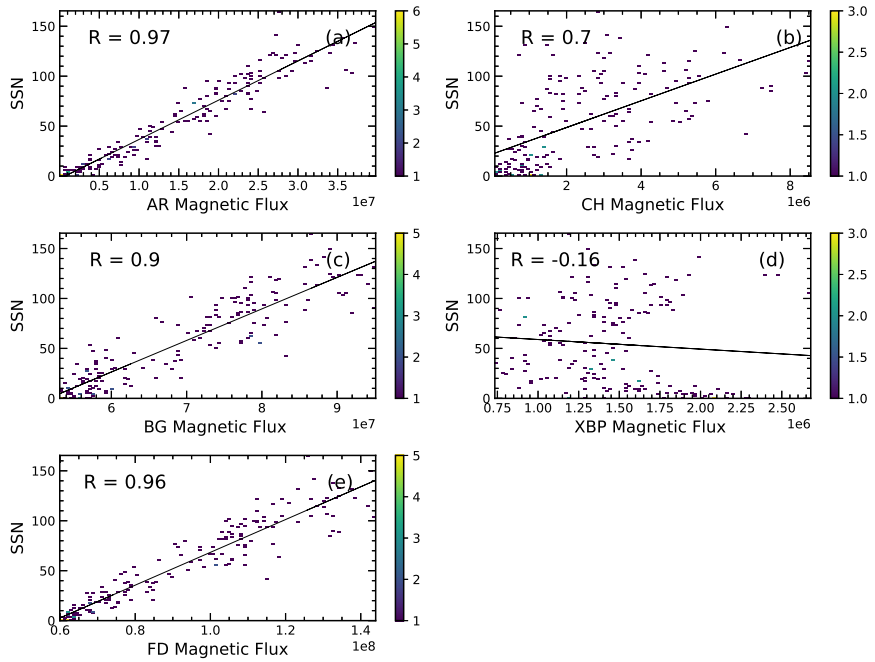

Figure 12. Total magnetic field of all the features: (a) ARs, (b) CHs, (c) BGs, (d) XBPs, and (e) FDT are plotted versus SSN for the period: May 01, 2010 to June 17, 2023 – after removing 27-day modulation.

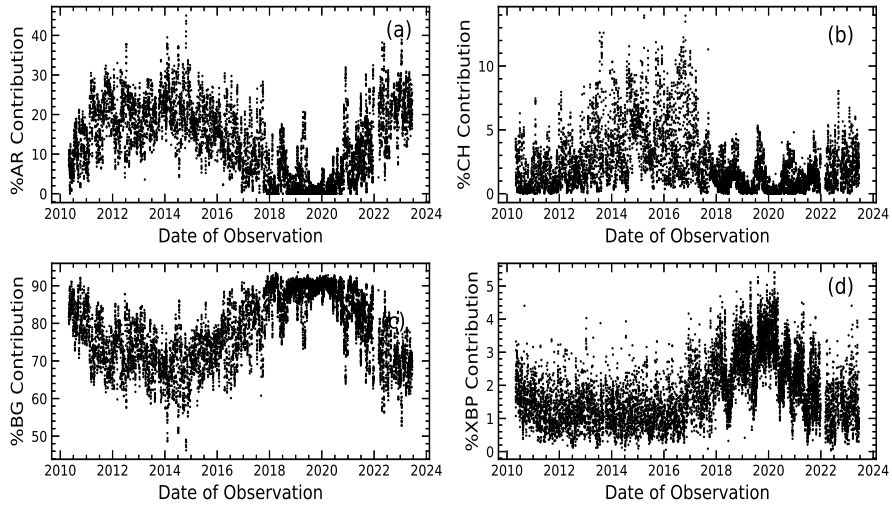

Figure 13. Variation of magnetic Contribution of ARs/CHs/BGs/XBPs to full-disk magnetogram (FDM) (a) ARs contribution variation, (b) CHs contribution variation, (c) BGs, and (d) XBPs contribution variations to full-disk magnetogram for the period: May 01, 2010 to June 17, 2023.

Table 3. Mean Magnetic flux density, Mean Magnetic flux density Contributions and Mean magnetic area of ARs/CHs/BGs/XBPs/FD

Feature	Mean Mag. Flux Density (DN) (Fig.5)	Mean Mag. Flux Density Contribution (%) (Fig.13)	Mean Magnetic Area (Number of Pixels) (Fig.7)
ARs	1.15×10^7	11.13	0.030×10^7
CHs	0.19×10^7	1.99	0.028×10^7
BGs	6.50×10^7	85.17	0.91×10^7
XBPs	0.15×10^7	1.99	0.014×10^7
FD	8.40×10^7	100	1.0×10^7

3.4. Magnetic Field Contributions of the Coronal Features

It is clear from Figures 5 and 6 that, on an average, over the solar cycle, the integrated magnetic flux density of BGs is larger than the integrated magnetic flux density of ARs/CHs/XBPs, but the contribution of ARs will become more prominent around solar maximum.

The full-disk magnetic flux density values does not reveal directly the contribution of different features, hence to determine the contribution of the segmented X-ray features to full-disk MFD, we used an expression:

$$MagneticFluxDensity\ \ Contribution\ \ (MFDC\ in\%) = \frac{(FM \times 100)}{FDM}$$

, where FM is feature's magnetic field integrated over its area and FDM is full-disk magnetic flux density.

The variations in the MFD contribution of all the X-ray coronal features (ARs/CHs/BGs/XBPs) to full-disk MFD variations are presented in Figure 13. Figure 13(a) and Figure 13(b) show that the MFD contribution of ARs and CHs vary in phase with the solar cycle, whereas the BGs and XBPs MFD contribution values, presented in Figure 13(c) and Figure 13(d), respectively, are opposite to the solar activity. The ARs and CHs occupies larger area during solar maximum, as a result less area available for XBPs and BGs, the area of BGs and XBPs reduce. Hence, we find that the variations in the MFD contributions for BGs and XBPs decrease as the sunspot number increases and whereas the MFD contributions for ARs and CHs are in phase with the solar cycle. The mean MFD, mean MFD contribution and mean magnetic area (number of pixels) values for all the features (ARs/CHs/BGs/XBPs/FD) are summarized in Table 3. We found that the mean MFD contribution estimated of the background regions (BGs) will be around 85.2 %, whereas ARs/CHs/XBPs are 11.1 %, 2.0 % and 2.0 % respectively to the average magnetic flux density of the full-disk for the period: 2010 - 2023.

Usually the ARs are more intense, high magnetic and brighter regions than other features, but they contribute less to the total surface magnetic field of the corona, because the ARs will be covered by less area over the full-disk compared

to BG regions (Figure 7 and Table 3). Whereas the BG regions contribute dominantly (about 85 %), simply because of the significant filling factor (large area) over the disk. Since the area of the features are different and are highly variable, they will have more impact on the total magnetic field variations.

4. Discussion and Conclusions

In this research work, we discussed in detail in using the XRT intensity maps of the coronal X-ray features and overlying on SDO/HMI full-disk magnetogram maps for the period from 2010 to 2023 (Solar Cycle 24). During this process, we have extracted the magnetic flux density of all the features (ARs/CHs/BGs/XBPs/FD) and studied their magnetic fluctuations. The variations in the magnetic field of a full-disk corona, and of all the features (ARs/CHs/BGs/XBPs) in comparison with intensity and temperature values and with SSN are presented. The main results of the full-disk intensity-temperature-magnetogram analysis are summarized as follows:

(i) The time series plots (shown in Figures 3, 4, 5 and 6) of the average magnetic flux density of the full-disk and all the features show magnetic fluctuations similar to intensity/temperature values and are synchronized with the solar cycle (sunspot number).

(ii) Although the magnetic flux density of all the features varies, but the mean magnetic flux density values estimated for the whole observed period of the full-disk is around $8.4\text{x}10^7$ DN, the active regions (ARs) will be around $1.15\text{x}10^7$ DN, whereas BGs, CHs, and XBPs are $6.5\text{x}10^7$ DN, $0.19\text{x}10^7$ DN, and $0.15\text{x}10^7$ DN, respectively.

(iii) It is evident from the Figure 13 and Table 3 that the background regions will have a greater impacts and large contribution to the average coronal magnetic field of the full-disk, up to 85 %, whereas the active regions contribute only up to 11 %. However, we observed that the contributions of CHs and XBPs are small, contributing approximately each about 2 % respectively, compared to BGs and ARs.

(iv) In addition, we found that the variations in the magnetic field contributions of ARs and CHs are in phase with the solar cycle, and whereas the magnetic field contributions of BGs and XBPs decrease as the sunspot number increases.

(v) The area of the ARs and CHs vary in phase with SSN, whereas the BGs and XBPs show an anti-correlation with SSN, as observed in Paper I also.

(vi) The area of the features are highly variable during their dynamical evolution, and they are responsible for the changes in the magnetic field values of the features.

(vii) The time series of the magnetic field of all the features (shown in Figures 5 and 6) show that the features are highly variable in their magnetic field similar to intensity/temperature fluctuations, suggesting that the magnetic field is crucial in producing the different emission features which are associated with different

intensity/temperature/magnetic field values. The magnetic field is responsible for the heating rate of the emission features which are highly variable on solar cycle timescales.

(viii) We conclude from the analysis that the magnetic field plays an important role in driving the different brightenings/emissions/temperature and heating of the corona at the sites of these magnetic features.

(ix) The automated identification and segmentation of the solar X-ray images and magnetograms are very useful in the reconstruction of the SSI variations.

(x) The combined investigations of the variations in intensity/temperature/magnetic field associated with all the coronal features will help to understand more clearly the corona's atmosphere and its heating mechanism.

Acknowledgements Hinode is a Japanese mission developed and launched by ISAS/JAXA, in collaboration with NAOJ as a domestic partner, NASA and STFC (UK) as international partners. The Hinode science team at ISAS /JAXA has conducted the Scientific operation of the Hinode mission. This team mainly consists of scientists from different institutes in the partner countries. JAXA and NAOJ (Japan), STFC (U.K.), NASA (U.S.A.), ESA, and NSC (Norway) have provided the support for the post-launch operation. The Hinode team had contributed all their efforts in the design, build, and operation of the mission. We also thank Solar Dynamic Observatory (SDO) of National Aeronautics and Space Administration (NASA) for providing HMI LOS magnetograms. RK and HNA wish to express their sincere thanks for the support received from ISEE/Nagoya University and SCOSTEP.

References

Adithya, H.N., Kariyappa, R., Shinsuke, I., Kanya, K., Zender, J., Damé, L., Gabriel, G., DeLuca, E., Weber, M.: 2021, Solar Soft X-ray Irradiance Variability, I: Segmentation of Hinode/XRT Full-Disk Images and Comparison with GOES (1 - 8 Å) X-Ray Flux. *Solar Phys.* **296**, 71. DOI. ADS.

Adithya, H.N., Kariyappa, R., Kusano, K., Masuda, S., Imada, S., Zender, J., Damé, L., Manjunath, H., DeLuca, E., Weber, M.: 2023, Solar Soft X-Ray Irradiance Variability, II: Temperature Variations of Coronal X-Ray Features. *Solar Phys.* **298**, 99. DOI. ADS.

BenMoussa, A., Gissot, S., Schühle, U., Del Zanna, G., Auchère, F., Mekaoui, S., Jones, A.R., Walton, D., Eyles, C.J., Thuillier, G., Seaton, D., Dammasch, I.E., Cessateur, G., Meftah, M., Andretta, V., Berghmans, D., Bewsher, D., Bolsée, D., Bradley, L., Brown, D.S., Chamberlin, P.C., Dewitte, S., Didkovsky, L.V., Dominique, M., Eparvier, F.G., Foujols, T., Gillotay, D., Giordanengo, B., Halain, J.P., Hock, R.A., Irbah, A., Jeppesen, C., Judge, D.L., Kretzschmar, M., McMullin, D.R., Nicula, B., Schmutz, W., Ucker, G., Wieman, S., Woodraska, D., Woods, T.N.: 2013, On-Orbit Degradation of Solar Instruments. *Solar Phys.* **288**, 389. DOI. ADS.

Couvidat, S., Schou, J., Hoeksema, J.T., Bogart, R.S., Bush, R.I., Duvall, T.L., Liu, Y., Norton, A.A., Scherrer, P.H.: 2016, Observables Processing for the Helioseismic and Magnetic Imager Instrument on the Solar Dynamics Observatory. *Solar Phys.* **291**, 1887. DOI. ADS.

Golub, L., Deluca, E., Austin, G., Bookbinder, J., Caldwell, D., Cheimets, P., Cirtain, J., Cosmo, M., Reid, P., Sette, A., Weber, M., Sakao, T., Kano, R., Shibasaki, K., Hara, H.,

Tsuneta, S., Kumagai, K., Tamura, T., Shimojo, M., McCracken, J., Carpenter, J., Haight, H., Siler, R., Wright, E., Tucker, J., Rutledge, H., Barbera, M., Peres, G., Varisco, S.: 2007, The X-Ray Telescope (XRT) for the Hinode Mission. *Solar Phys.* **243**, 63. DOI. ADS.

Hoeksema, J.T., Liu, Y., Hayashi, K., Sun, X., Schou, J., Couvidat, S., Norton, A., Bobra, M., Centeno, R., Leka, K.D., Barnes, G., Turmon, M.: 2014, The Helioseismic and Magnetic Imager (HMI) Vector Magnetic Field Pipeline: Overview and Performance. *Solar Phys.* **289**, 3483. DOI. ADS.

Kosugi, T., Matsuzaki, K., Sakao, T., Shimizu, T., Sone, Y., Tachikawa, S., Hashimoto, T., Minesugi, K., Ohnishi, A., Yamada, T., Tsuneta, S., Hara, H., Ichimoto, K., Suematsu, Y., Shimojo, M., Watanabe, T., Shimada, S., Davis, J.M., Hill, L.D., Owens, J.K., Title, A.M., Culhane, J.L., Harra, L.K., Doschek, G.A., Golub, L.: 2007, The Hinode (Solar-B) Mission: An Overview. *Solar Phys.* **243**, 3. DOI. ADS.

Kumara, S.T., Kariyappa, R., Zender, J.J., Giono, G., Delouille, V., Chitta, L.P., Damé, L., Hochedez, J.-F., Verbeeck, C., Mampaey, B., Doddamani, V.H.: 2014, Segmentation of coronal features to understand the solar EUV and UV irradiance variability. *Astron. Astrophys.* **561**, A9. DOI. ADS.

Pevtsov, A.A., Fisher, G.H., Acton, L.W., Longcope, D.W., Johns-Krull, C.M., Kankelborg, C.C., Metcalf, T.R.: 2003, The Relationship Between X-Ray Radiance and Magnetic Flux. *Astrophys. J.* **598**, 1387. DOI. ADS.

Skumanich, A., Smythe, C., Frazier, E.N.: 1975, On the statistical desription of inhomogeneities in the quiet solar atmosphere. I. Linear regression analysis and absolute calibration of multichannel observations of the Ca^{+} emission network. *Astrophys. J.* **200**, 747. DOI. ADS.

Takeda, A., Yoshimura, K., Saar, S.H.: 2016, The Hinode/XRT Full-Sun Image Corrections and the Improved Synoptic Composite Image Archive. *Solar Phys.* **291**, 317. DOI. ADS.

Zender, J.J., Kariyappa, R., Giono, G., Bergmann, M., Delouille, V., Damé, L., Hochedez, J.-F., Kumara, S.T.: 2017, Segmentation of photospheric magnetic elements corresponding to coronal features to understand the EUV and UV irradiance variability. *Astron. Astrophys.* **605**, A41. DOI. ADS.